PHILOSOPHICAL TRANSACTIONS OF THE ROYAL SOCIETY A MATHEMATICAL, PHYSICAL & ENGINEERING SCIENCES

Observations of the Semidiurnal Internal Tide in the Western North Atlantic Ocean

R. M. Hendry

Phil. Trans. R. Soc. Lond. A 1977 **286**, 1-24
doi: 10.1098/rsta.1977.0108

OBSERVATIONS OF THE SEMIDIURNAL INTERNAL TIDE IN THE WESTERN NORTH ATLANTIC OCEAN

By R. M. HENDRY
Institute of Oceanographic Sciences, Wormley, Surrey, England

(*Communicated by H. Charnock, F.R.S. – Received 25 May 1976*)

Extensive moored measurements of temperature and horizontal current fluctuations in a Mid-Ocean Dynamics Experiment in the deep western North Atlantic near 28° N, 70° W are analysed for semidiurnal tides. The M_2 principal lunar tide is dominant, and about 50 % of the main thermocline temperature variance in the M_2 band is coherent with the astronomical forcing and so of a deterministic rather than random nature. The first baroclinic mode is dominant in the internal tide, and propagates to the southeast through the experimental area. The M_2 first mode internal tide has an energy density of 0.9×10^2 J/m^2, about 20 % as great as the barotropic tide energy density, and the horizontal currents in the barotropic and baroclinic tides are comparable with a characteristic deep amplitude of 1 cm/s. It is proposed that the Blake Escarpment 700 km to the west is a major generation area for the internal tide, and simple theoretical arguments suggest that the Escarpment is especially effective in generating low mode internal waves. Neighbouring tidal bands are much more dominated by randomly phased internal waves, but the S_2 principal solar band shows evidence for a weak deterministic internal tide. Mooring motion adds incoherent noise to the tidal period temperature fluctuations. Barotropic currents for the major M_2, S_2 and N_2 semidiurnal constituents are derived from the current measurements, although internal wave noise levels are high.

1. Introduction

Internal gravity waves are an important source of current, temperature and salinity variance in the oceans. Internal tides are internal waves with astronomical tidal periods, owing their existence to the forcing of the Sun and Moon. Early work (Zeilon 1934) showed that continental slopes or other topography could interact with a depth independent motion, such as a barotropic tide, to produce internal waves with a depth dependent structure. Since the beginning of the study of oceanic internal tides, dating perhaps from Nansen (1902), observations from coastal areas have been more comprehensive than those from the deep ocean, where practical considerations restricted observations. Some early studies are reviewed by Defant (1949). Seiwell (1942) and Haurwitz (1952) reported on limited observations of semidiurnal internal tides in the Atlantic Ocean, but Haurwitz emphasized that some of the harmonic analyses of his short temperature time series did not differ significantly at the tidal frequencies from what might be obtained in a similar analysis of random noise. This showed that statistical considerations were important in characterizing oceanic internal tides. A modern review of internal tides is given by Wunsch (1975).

In this work, we examine the semidiurnal internal tides in the western North Atlantic at the site of the Mid-Ocean Dynamics Experiment (MODE-1) during the first half of 1973. The MODE observations were unique in their open ocean setting and quantity of data. For the

first time, a real demonstration of determinism in the deep ocean internal tide is possible, and a rare cause and effect relationship in internal wave motions is revealed. The extensive observations from MODE-1 provide reliable statistics, and allow a description of the energy content, bandwidth and persistence of the internal waves comprising the semidiurnal peak in the energy spectrum. Propagation characteristics of the fields can be derived, and related to energy sources. Section 2, following, summarizes the experimental setting and analysis techniques.

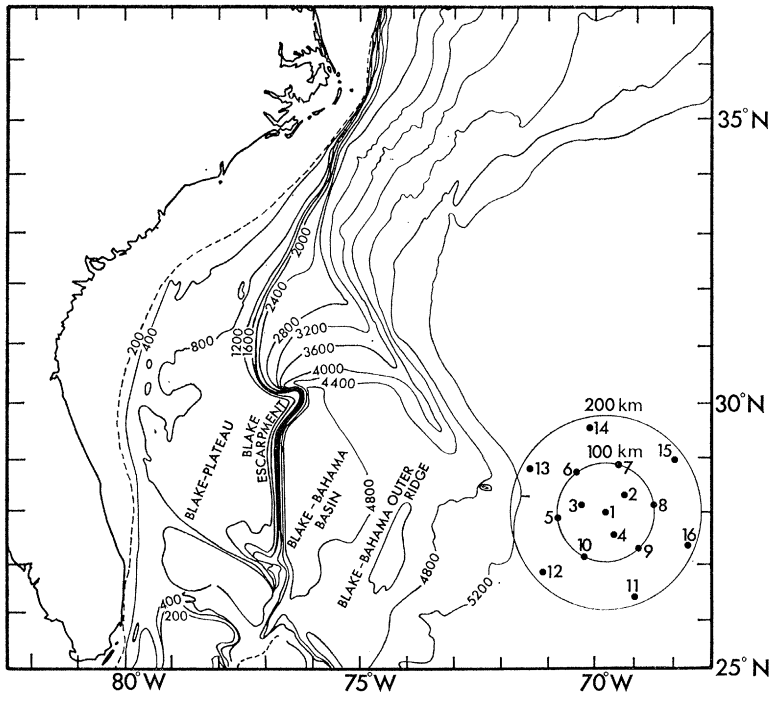

FIGURE 1. Chart of the MODE area, showing the array of fixed moorings. Bathymetric contours in metres.

Section 3 deals with average energy in the semidiurnal current and temperature fluctuations, and Section 4 discusses evidence for a deterministic internal tide at the MODE-1 site. Some results for the barotropic tidal current fields are also presented. Section 5 contains a discussion of the generation problem relating to the MODE-1 observations, and §6 considers mooring motion. The conclusions of the study are reviewed in §7. This report is based on thesis work completed recently by the author (Hendry 1975).

2. SETTING, DATA AND ANALYSIS

The Mid-Ocean Dynamics Experiment (MODE Scientific Council, 1973) affords a unique look at deep ocean physics. The experiment was designed to investigate mesoscale oceanic circulation, but the observations are valuable for internal wave studies as well. Horizontal current, temperature and pressure time series were obtained from instruments on sixteen fixed moorings, with sub-surface flotation, centred at 28° N latitude and 70° W longitude and largely over a smooth abyssal plain at 5400 m depth. The moorings were arranged in three concentric circles, with radii 50, 100 and 180 km, and a highly instrumented mooring in the centre of the pattern. With the nearest large topographic features the Blake Escarpment 700 km

to the west and the Mid-Atlantic Ridge over 2000 km to the east, the experiment is in the far field of any likely major internal tide generation area. Figure 1 gives an overall view of the experimental area, showing the array of fixed moorings. The moorings were instrumented with Savonius rotor current meters, the majority of vector-averaging type recording temperature as well as horizontal currents. Temperature and pressure (*T-P*) recorders (Wunsch & Dahlen 1974) were also used on the moorings, with the pressure measurements monitoring the vertical motion of the moorings. Nominal depth levels of 400, 700, 1400, 3000, 4000 and 5000 m were instrumented with temperature recording current meters, while 500, 900, 1100, 1900, 2700, 3700 and 4700 m depth levels had *T-P* coverage. Most temperature records lasted for at least 75 days, with a group extending over 105 days, and all moorings except one had a minimum of four levels instrumented for temperature. The current measuring programme was less successful due to instrumental problems (Dexter, Milliman & Schmitz 1975), and many of the 50 usable records were quite short. The four month MODE-1 field programme gave about 27 record-years of temperature measurements and 6 record-years for currents.

The data were analysed for tides in a consistent manner, with all records broken into 15 day non-overlapping lengths. Each such length of north or east current components, temperature or pressure time series had its mean value subtracted out, and was then multiplied by a cosine tapering window over the first and last 10 % of the record to reduce end effects. Fourier transforms of the resulting time series were computed and the Fourier coefficients corrected for the amplitude reduction due to the tapering. For each 15-day piece, a parallel time series of the equilibrium astronomical tide at the measuring point was generated and harmonically decomposed using the same techniques, to allow estimates of the admittance of the physical fields with respect to the equilibrium tide (Wunsch 1972). The semidiurnal frequency band is covered by three adjacent Fourier coefficients at periods of 12.86, 12.41 and 12.00 h and separated by a bandwidth of $\frac{1}{15}$ cycle per day. These will be referred to as the N_2, M_2 and S_2 bands respectively, since the astronomical tides designated by these symbols dominate the equivalent bands of the equilibrium tide. Once the raw Fourier coefficients were obtained, we estimated the energy at different depths and in different frequency bands by averaging over the appropriate ensembles. For long-enough records from individual instruments, we estimated the coherence between the physical processes and the equilibrium tide by averaging over consecutive pieces to determine if the internal waves were simply related to the tidal forcing. The fluctuations coherent with the astronomical forcing were analysed for spatial variations, both vertical and horizontal, to see if a wave-like character could be detected in the fields. At an individual mooring, the vertical variations in amplitude and phase of the coherent motion could be least-squares fitted to a limited set of normal modes calculated from internal wave theory, and an individual mode analysed for horizontal variation. The MODE-1 array was designed to be an effective antenna for detecting horizontal wave motion; although the spatial scales of internal waves may be different from those of mesoscale eddies, in our case the array proved adequate for the internal tide. For the modal analysis, the temperature fluctuations were converted to isotherm depth fluctuations by dividing by the measured local potential temperature gradient. Since the highest level sampled in the experiment was at 400 m depth, only two or three baroclinic modes could be used without aliasing energy of low mode origin into higher modes, which vary rapidly near the surface but resemble lower order modes at depth. The modes used in the fits were always the gravest ones, and with the MODE-1 data the procedure gives reasonable results for the temperature field. For the currents, little averaging is possible

PHILOSOPHICAL TRANSACTIONS OF THE ROYAL SOCIETY A MATHEMATICAL, PHYSICAL & ENGINEERING SCIENCES

because of the shortness of the records, but we can treat some individual cases. The pressure time series were analysed to determine the apparent temperature variance due simply to mooring motion, and the effects of this contamination on conclusions about the internal tides.

3. Energy variation with depth and frequency

To estimate the energy in the semidiurnal frequency band, we averaged observations at a given depth from all points in the array, and over the duration of the experiment. The processes involved are broadly stationary in time and horizontal location, but show structure in the vertical and in frequency space which we examined more stably by the averaging.

Figures 2*a*, *b*, *c* show resulting average profiles of squared temperature fluctuation amplitude for the three semidiurnal bands (ensemble averages of squared amplitude, not time averages of squared fluctuations). Figure 2*a* gives the number of 15-day pieces in averages at each depth, and standard 95 % error bars for the 3500 m level which had the fewest pieces. The standard error bars for the points with the largest number of samples are indistinguishable from the points themselves, but these error estimates are based on a model of a random time series, where individual pieces are independent, which is violated for a partially deterministic process. The central M_2 frequency band dominates the adjacent semidiurnal bands by a factor of three in energy throughout the water column except at the deepest level. There the M_2 and S_2 estimates are about equal, with the N_2 estimate still lower by the factor of three. The bands on either side of the M_2 estimate have remarkably similar energy levels with the exception of this lowest depth. This would be expected if the adjacent bands were dominated by M_2 energy, Doppler shifted symmetrically in frequency space by random low frequency currents: in terms of the relation

$$\Delta\sigma = \boldsymbol{k}\cdot\boldsymbol{U}$$

relating frequency shift $\Delta\sigma$ to wavenumber $\boldsymbol{k}$ and a mean current $\boldsymbol{U}$, a shift of a first mode M_2 internal wave of wavelength 160 km by $\frac{1}{15}$ c/d would result from a 10 cm/s mean flow. In the ocean, a realistic treatment must relate the statistical observation that the M_2 peak has a bandwidth of at most $\pm\frac{1}{15}$ c/d to its $\frac{1}{3}$ power points, to the statistics of the internal tide and the fluctuating depth dependent low frequency fields, if these were known.

The same averaging by depth levels was done for current components at the three semidiurnal frequencies, as shown in Figures 3*a*, *b* and *c*. The number of pieces involved in each average and 95 % error bars for the level with fewest samples are included in figure 3*a*. Since the horizontal currents include both barotropic and baroclinic components, the vertical distribution of horizontal kinetic energy does not reflect only the internal wave field and more information is needed to separate the two effects. The M_2 band is dominant in horizontal kinetic energy as well as temperature variance, with about five times more energy above 1500 m and nearly a decade more in the deeper water than the adjacent frequency bands. The nominal S_2 and N_2 bands show comparable energies at each depth, but with more scatter than seen in the temperature variance profiles. The M_2 horizontal kinetic energy below 1400 m is quite constant with depth, suggesting an energetic barotropic component of the currents, while the adjacent frequencies show more vertical variations in energy. The baroclinicity of the N_2 and S_2 current profiles suggests that much of the energy in these bands is derived from internal waves, being either Doppler shifted M_2 frequency energy or simply part of the non-tidal internal wave continuum. These remarks can be amplified when we discuss estimates of the actual barotropic

current components in the three semidiurnal bands. Looking ahead, we indicate in figures 3*a*, *b* and *c* estimates of the barotropic energy for the three bands, noting the relatively unenergetic barotropic currents in the N_2 and S_2 bands compared to the overall currents.

For comparison of the overall averages with some theoretical notions of internal gravity waves, figures 4*a* and *b* give vertical profiles of $N^{-1}(z)\,(\mathrm{d}\theta/\mathrm{d}z)^2$ and $N(z)$, where N is the Brunt–Vaisala frequency and θ potential temperature for the MODE-1 site from average hydrographic data in the experiment. An approximate theory, valid for an internal wave field composed of a random mixture of high modes far from vertical or horizontal boundaries (see,

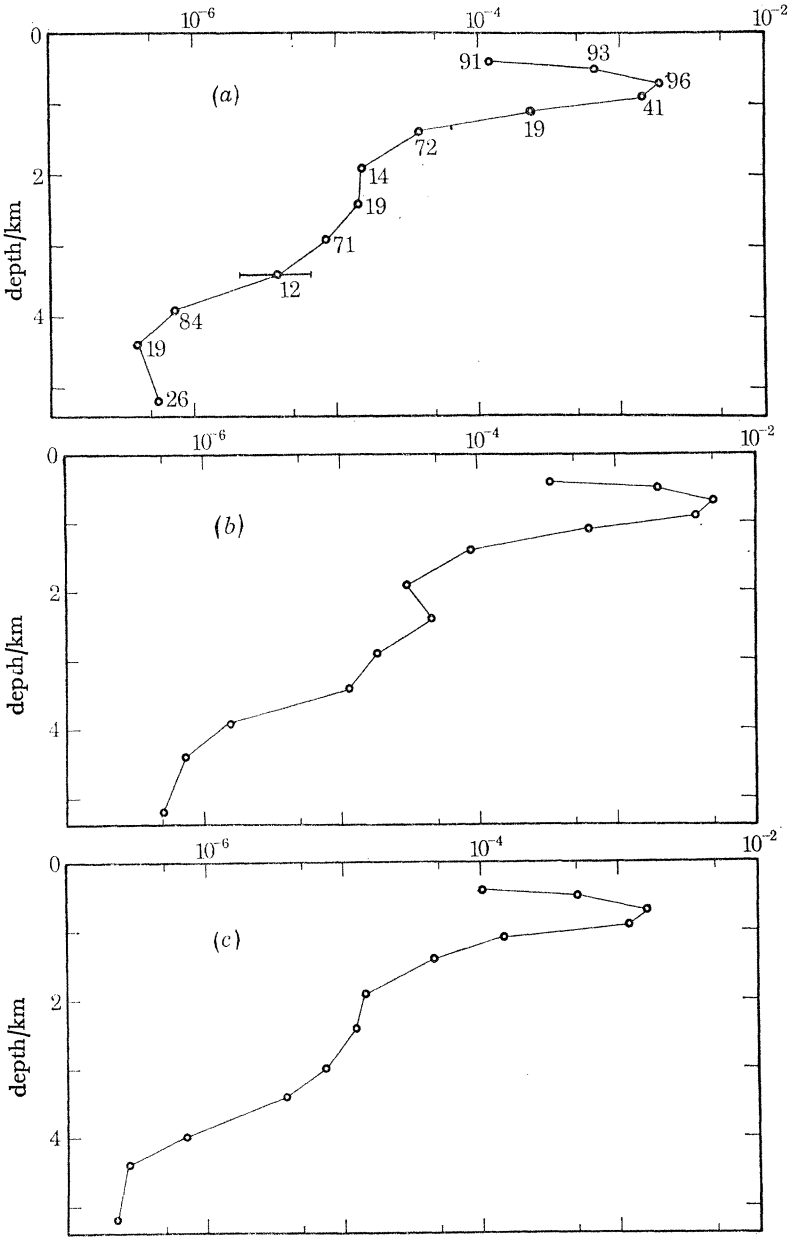

FIGURE 2*a*. Vertical profile of squared temperature fluctuations in the S_2 band (°C²), averaged at depth levels over the entire array. The number of 15-day piece lengths at each level is indicated.

FIGURE 2*b*. Vertical profile of average squared temperature fluctuations in the M_2 band.

FIGURE 2*c*. Vertical profile of average squared temperature fluctuations in the N_2 band.

for example, Munk & Phillips 1968) shows that the vertical structure of, respectively, temperature variance and horizontal kinetic energy will follow these expressions. Departures of the observations from these derived profiles will indicate that not all of the necessary assumptions are fulfilled. For the profiles of temperature variance, all three semidiurnal frequency bands show a general similarity to the profile of $N^{-1}(\mathrm{d}\theta/\mathrm{d}z)^2$, notably in the sharp maximum at 750 m in the main thermocline and the slight inflexional feature between 2000 and 3000 m. However,

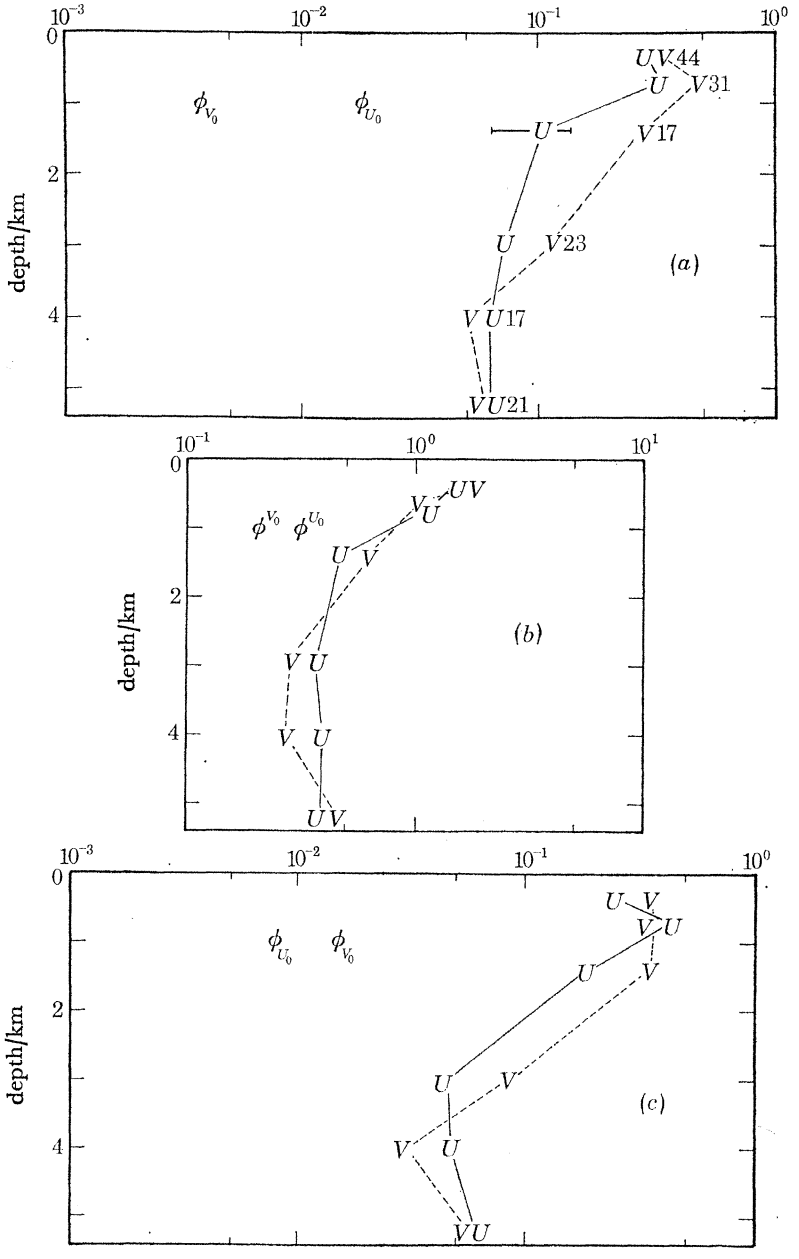

FIGURE 3*a*. Vertical profile of squared horizontal current ((cm/s)^2) for U (east) and V (north) in the S_2 band, averaged at depth levels over the entire array. Estimates of squared amplitude for the barotropic current components U_0 and V_0 are given, showing that the currents are dominated by internal waves at all depths.

FIGURE 3*b*. Similar estimates for the M_2 band currents. Here the deep currents are greatly influenced by the barotropic mode.

FIGURE 3*c*. Similar estimates for the N_2 band. Internal waves appear to dominate at all depths.

there is more global variation in the vertical profiles of temperature variance than the derived profile: the thermocline values are larger or the deep ocean values smaller than a fit by the theoretical curve, by almost an order of magnitude for the M_2 band and by about a factor of five for the adjacent bands. This is consistent with internal wave fields involving energetic low order modes, whose vertical structure is not so closely governed by the local density gradients as the geometrical optics theory demands.

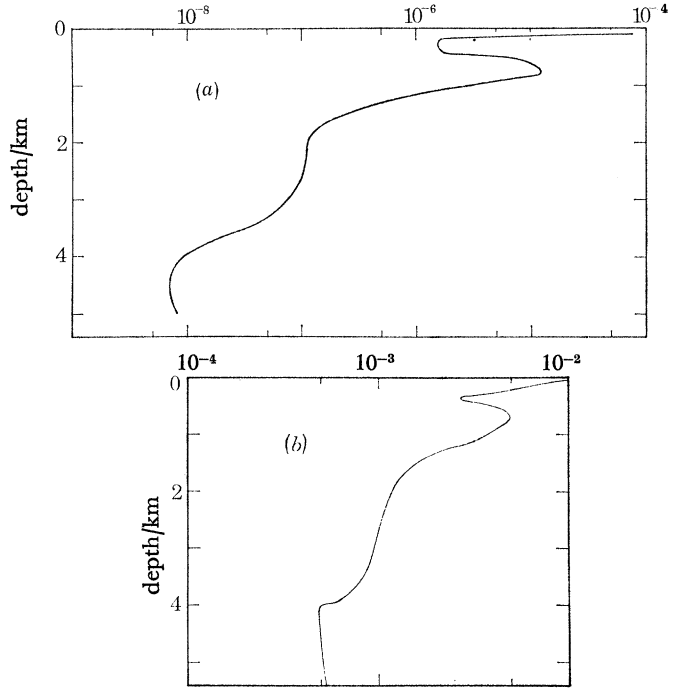

FIGURE 4*a*. Vertical profile of $N^{-1}(z)(\mathrm{d}\theta/\mathrm{d}z)^2$ from average MODE hydrography, where N is Brunt–Vaisala frequency and θ potential temperature. The vertical distribution of temperature variance in a field of high mode randomly phased internal waves should be similar to the profile.

FIGURE 4*b*. Vertical profile of $N(z)$ from average MODE hydrography. The profile will be similar to the vertical distribution of average horizontal kinetic energy in an idealized field of high mode internal waves.

The $N(z)$ profile of figure 4*b* shows a thermocline maximum and deep water values less by an order of magnitude. This behaviour is mirrored in the profiles of squared horizontal current for the S_2 and N_2 bands, figures 3*a* and *c*, but not as much by the M_2 profile of figure 3*b*. Any departure of the adjacent bands from the random, high mode internal wave field model is not as apparent in the average current profiles as it was in the profiles of temperature variance, where small deviations are magnified by essentially the third power of $N(z)$ rather than the first power. For the central M_2 band, we have already noted the near constant energy levels in the deeper water due to the barotropic tide.

Table 1 records estimates of the depth integrated horizontal kinetic energy, vertical potential energy and total energy in the three frequency bands. The average potential energy in fluctuations at a given depth is

$$\tfrac{1}{4}N^2(z)\zeta^2(z),$$

where

$$\zeta = -T/(\mathrm{d}\theta/\mathrm{d}z)$$

is isopycnal displacement, derived from measured temperature fluctuation amplitude T and the local vertical gradient of potential temperature, and the assumption of a perfect temperature-salinity correlation. Table 1 shows the dominance of the M_2 band and the remarkable equality of energy levels in the adjacent bands. Although the baroclinic motions in these adjacent bands may be dominated by energy shifted from the central M_2 peak, we will derive estimates of the barotropic currents in each of the bands, and the next section presents evidence for a true S_2 internal tide.

TABLE 1. ESTIMATES OF THE DEPTH INTEGRATED HORIZONTAL KINETIC ENERGY AND POTENTIAL ENERGY IN TIDAL PERIOD FLUCTUATIONS FOR THE THREE SEMIDIURNAL BANDS, AND RESULTING TOTAL ENERGY DENSITIES: THE M_2 BAND DOMINATES AND THE EQUALITY OF THE ENERGY LEVELS IN THE ADJACENT BANDS IS REMARKABLE

band	central frequency / cycles/h	horizontal kinetic energy / J/m²	potential energy / J/m²	total / J/m²
N_2	0.0777	0.50×10^2	0.25×10^2	0.75×10^2
M_2	0.0806	0.18×10^3	0.98×10^2	0.28×10^3
S_2	0.0833	0.47×10^2	0.25×10^2	0.72×10^2

4. DETERMINISTIC MOTION IN THE TIDAL BAND

When enough data from a given instrument was available, an attempt was made to project the tidal frequency fluctuations onto the equilibrium tide. In frequency space, this assumed a model

$$\hat{T} = \hat{a}\hat{\xi}_e + \hat{r},$$

where $\hat{T}$ is, for example, the Fourier transform of temperature fluctuations at a tidal frequency, $\hat{\xi}_e$ the transform of the equilibrium tide, and $\hat{a}$ an admittance function relating the two. $\hat{r}$ is uncorrelated noise. This is the most general linear and local relation between the physical fields and the tidal forcing. Although it is not suggested that the internal tides are generated directly by the gravitational forcing, the barotropic tides which provide the energy for the internal tides are simply related to the forcing and the admittance function $\hat{a}$ implicitly acknowledges this. Given an ensemble of Fourier coefficients of temperature and equilibrium tide, and denoting an ensemble average by $\langle\ \rangle$, we can estimate the deterministic part of the measured fields. The phases of each raw Fourier coefficient are referred to the time origin of the particular component of the equilibrium tide, so becoming admittance phases. Then a simple average

$$\langle\hat{T}\rangle = \langle\hat{a}\hat{\xi}_e\rangle$$

estimates the true tidal signal. The coherence between the signal and the equilibrium tide is defined as

$$C = \langle\hat{T}\hat{\xi}_e^*\rangle / \langle\hat{T}\hat{T}^*\rangle^{\frac{1}{2}}\langle\hat{\xi}_e\hat{\xi}_e^*\rangle^{\frac{1}{2}},$$

where $\hat{T}^*$ is the complex conjugate of $\hat{T}$, so C^2 is the fraction of the total energy in the signal which can be related to the equilibrium tide by the admittance $\hat{a}$. We are faced with the problem of estimating $\hat{a}$ from a limited number of observations, and the statistics of the distribution of C when the true value of $\hat{a}$ is zero provide a guide for interpreting the results.

For the M_2 tides, we first describe the results from the temperature measurements. Most temperature records gave either five or seven 15-day pieces, and averages over these pieces showed a highly significant coherence between the M_2 temperature fluctuations and the M_2 equilibrium tide. This is an interesting result, since it means that part of the internal wave motion in this band in the MODE-1 area is predictable just as the barotropic tide is subject to prediction. In table 2, we show the results for the heavily instrumented central mooring as illustration. The ensemble averages of M_2 maximum isotherm displacement as a function of

TABLE 2. AVERAGE M_2 ISOTHERM FLUCTUATIONS FROM TEMPERATURE RECORDS ON THE CENTRAL MOORING, GIVING AMPLITUDE AND GREENWICH EPOCH G, AS A FUNCTION OF DEPTH

(Estimates of coherence amplitude of the temperature fluctuations and the equilibrium tide, with 7 degrees of freedom, are also given. For true coherence of zero, 95 % of such estimates would be less than 0.63. The admittance phase is sensibly constant with depth, showing that isothermal surfaces are tending to rise and fall in phase throughout the water column.)

depth/m	amplitude/m	phase/°G	coherence
389	1.52	022	0.57
391	1.56	023	0.58
489	1.41	011	0.68
490	1.46	022	0.68
691	1.93	355	0.76
697	1.97	004	0.75
897	2.69	349	0.69
1095	3.42	356	0.69
1392	2.05	004	0.50
1895	3.13	353	0.52
2399	3.74	025	0.50
2916	5.03	006	0.64
2919	4.86	018	0.64
3437	4.85	023	0.63
4382	1.98	006	0.39
5348	1.45	017	0.28

depth, the admittance phase (Greenwich epoch G) and estimates of coherence amplitude are given, for averages over seven individual pieces. For seven degrees of freedom, if the true admittance is zero the expected value of the estimated coherence is 0.34, while 95 % of all such estimates are less than 0.63 (Amos & Koopmans 1963). For a true coherence of 0.7 and 7 degrees of freedom, the phase estimates have 95 % error bars of almost $\pm 40°$; from table 2 we also see that the phase of the M_2 isotherm displacement is essentially constant with depth, although the coherence amplitudes and resulting phase error bars do vary with depth. This vertical structure is characteristic of a dominant first baroclinic mode, and the maximum coherences also occur in the main thermocline where the first mode has its maximum amplitude. In a least-squares fit of the distribution of amplitudes and phases in table 2 by the first three internal wave modes calculated from the average hydrography, 93 % of the total variance was accounted for, and of this 84 % was contained in the first baroclinic mode. A third baroclinic mode with 12 % of the fitted variance accounts for the large amplitudes near 3000 m, but the density stratification is small there and the resulting fluctuations in potential energy similarly small. The phases of the deeper levels should be dominated by this third mode, so the absolute constancy of admittance phases throughout the water column is partly coincidental at the central mooring.

As an overview of the predictability of the internal tide in the MODE-1 area, figure 5 gives vertical profiles of average coherence amplitude between temperature fluctuations and the

PHILOSOPHICAL TRANSACTIONS OF THE ROYAL SOCIETY A MATHEMATICAL, PHYSICAL & ENGINEERING SCIENCES

equilibrium tide for the three semidiurnal frequency bands. Cases with both 5 and 7 degrees of freedom were included, and figure 5 shows the expected value of the coherence estimates for a random temperature field for each case for comparison. Finite coherence estimates are positively biased, with the bias depending on the true coherence and the number of degrees of freedom. The true predictable fraction of power must be estimated by the unbiased coherence squared, for which an approximation is

$$C^2 = (N\hat{C}^2 - 1)/(N-1)$$

with $\hat{C}$ the finite estimate and N the number of degrees of freedom (Munk & Cartwright 1966).

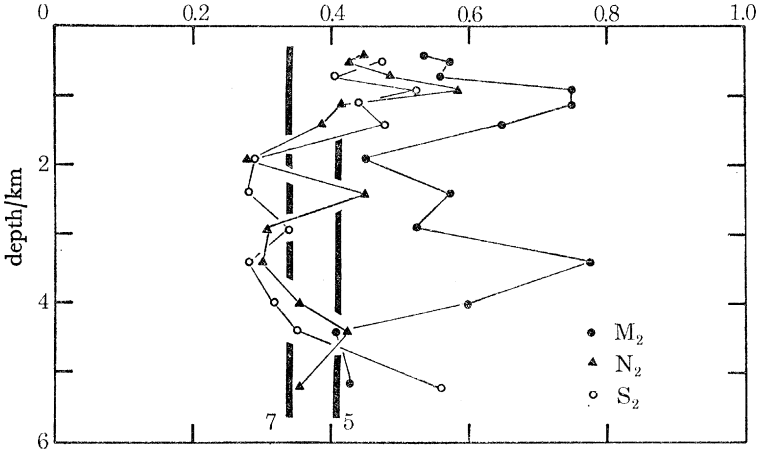

FIGURE 5. Vertical profile of average coherence amplitude of temperature fluctuations and the equilibrium tide for three semidiurnal frequency bands. The averages are taken over the whole array at depth levels, and include individual cases with both 5 and 7 degrees of freedom. The expected values of coherence amplitude for zero true coherence are shown for each case, and while the central M_2 band shows a definite determinism, the adjacent frequency bands are much more dominated by randomly phased temperature fluctuations.

The bias will be unchanged by averaging a number of finite coherence estimates together as we have done, but the variance of the estimators will be reduced. The M_2 frequency band shows a significant determinism in the temperature field down to 4000 m, but the temperature fluctuations at the deeper levels are not significantly different from random noise. For the N_2 and S_2 bands, the temperature fluctuations give average coherences with the equilibrium tide generally not different from what we would expect for random noise, with the exception of an indication at 900 m of higher coherence which mirrors the maximum in the M_2 coherence profile. For the M_2 temperature fluctuations near the main thermocline, coherences near 0.7 indicate that about 50 % of the temperature variance is predictable. In figure 5, the M_2 coherence amplitudes in the depths between 3000 and 4000 m show a possible secondary maximum, and at least show a distinctly different behaviour from that of the N_2 and S_2 bands where the temperature-equilibrium tide coherences are uniformly low. This structure in the M_2 fluctuations could be due to persistent higher order modes, with displacement maxima in the deeper water as well as in the main thermocline. The third baroclinic mode, with a displacement maximum at about 3150 m depth, did show some energy in the central mooring modal decomposition, but the lack of vertical resolution on most of the moorings prevents much further analysis of the higher modes. Noble (1975) has discussed some observations in the same region of the Atlantic which can be interpreted as showing higher mode internal tides persisting over many weeks, but our results indicate that at least in the main thermocline the first baroclinic mode is dominant.

Although some of the other moorings which we analysed from MODE-1 have as few as four temperature sensors for vertical resolution, the results from the central mooring suggest that fits with a limited number of normal modes will give meaningful results. Visually, most of the other moorings showed very stable M_2 admittance phases as a function of depth for the temperature fluctuations. To examine the horizontal structure in the M_2 tide, only fourteen of the sixteen moorings were used finally, since one mooring as mentioned had insufficient vertical coverage,

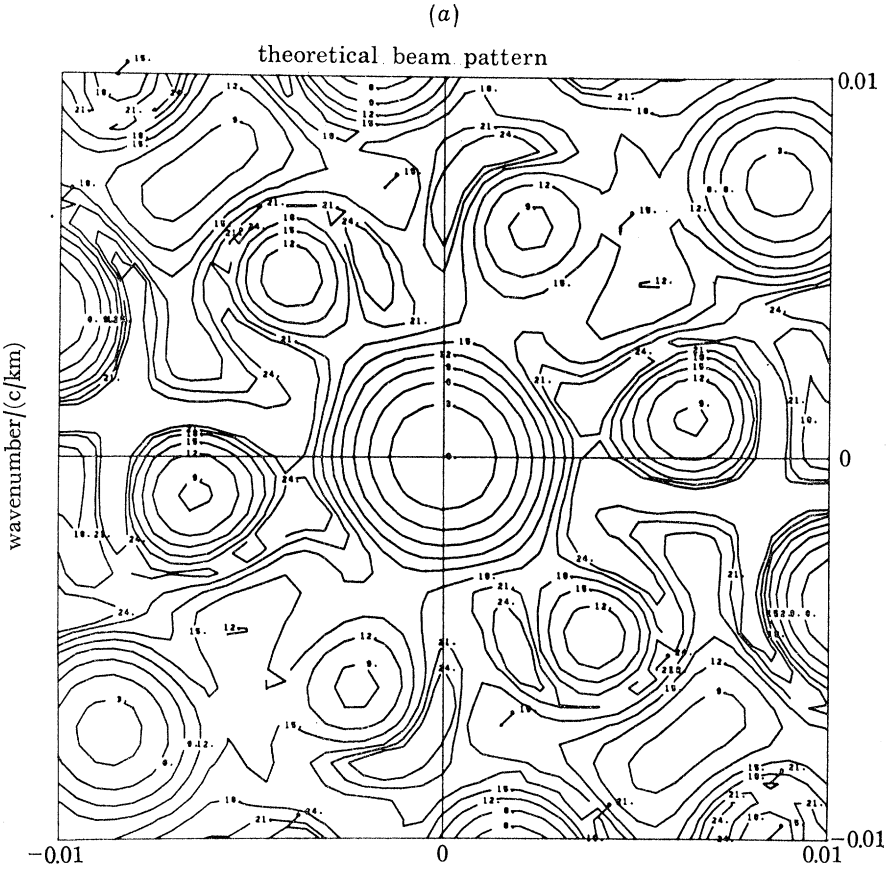

FIGURE 6*a*. The theoretical beampattern for the 14-point array used in the horizontal wavenumber analysis. The contours are logarithmic, with separation −3 dB, and the pattern is normalized by its maximum value. A noise-free plane wave incident on the array would give the beampattern centered about the incident wavenumber in a conventional wavenumber spectrum analysis. Note the sidelobes of the main peak at the first alias with wavenumber about 1/100 cycle/km, corresponding to the 50 km closest spacing of points in the array.

and measurements from one other mooring seemed dominated by mooring motion. This will be discussed in §6 which deals with the pressure measurements. The three lowest order baroclinic modes were used in a least-squares fit of the temperature fluctuations on these fourteen moorings, and the fits were repeated with only the first two modes as a test of stability. In only one case was there a significant change, as one of the moorings with only four points in the vertical and an almost constant admittance phase with depth showed a dominant third mode signal when three modes were used, a result of aliasing. For this mooring in particular, the first baroclinic mode was estimated by the two mode fit. Among the fourteen moorings, between 68 and 98% of the vertically summed temperature variance was accounted for in the fits, and in these fits the first baroclinic mode accounted for between 75 and 99% of the energy.

With the derived amplitudes and phases of the first baroclinic modes, our viewpoint can shift from local to global. Using the array as a horizontal antenna, we computed estimates of the horizontal wavenumber spectrum in the first mode M_2 temperature fluctuations. Since the nominal separation of points in the array is about 50 km, waves with horizontal wavelengths less than about 100 km will be near aliases of longer waves as perceived by the antenna. Figure 6*a* shows the beam pattern $B(k)$ of the array (Capon 1969), defined as a function of horizontal wavenumber $\boldsymbol{k} = (kx, ky)$ by the expression

$$B(\boldsymbol{k}) = (1/M)^2 \sum_{p=1}^{M} \sum_{q=1}^{M} \exp i\boldsymbol{k}\cdot(\boldsymbol{X}p - \boldsymbol{X}q),$$

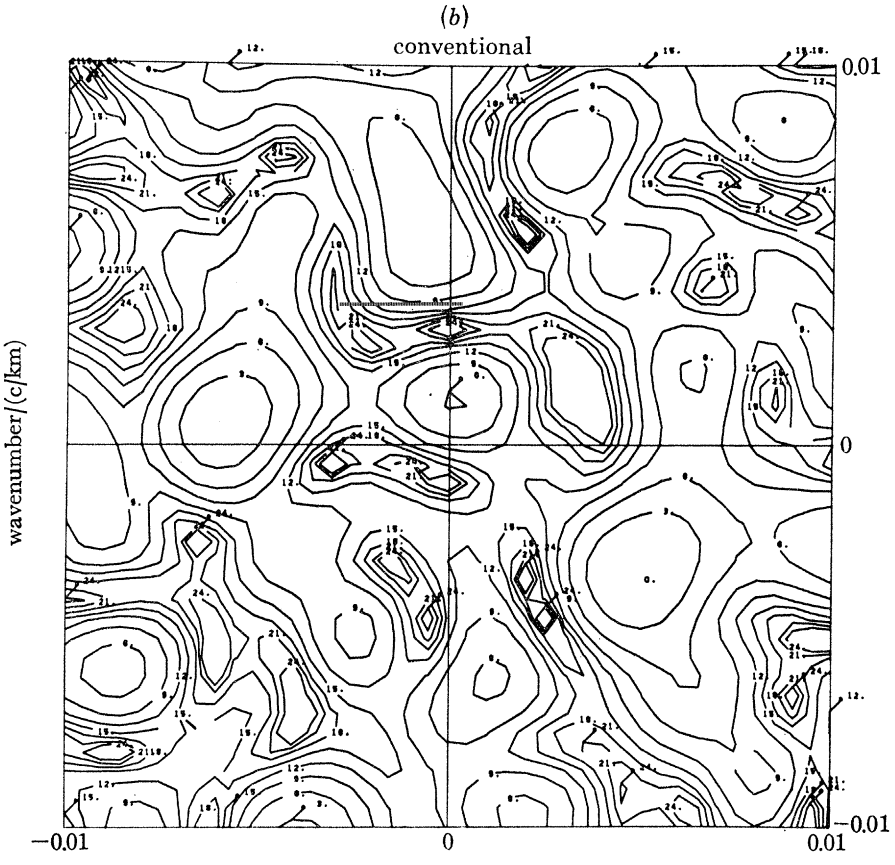

FIGURE 6*b*. Conventional wavenumber spectrum of first mode M_2 temperature fluctuations from MODE. The peak in the southeast quadrant has wavenumber 1/163 cycle/km and represents a wave propagating from northwest to southeast. A secondary peak in the northwest quadrant is interpreted as an alias of the main peak.

where $\boldsymbol{X}p$, $p = 1, M$ is the horizontal location of the pth point in the M point array. The conventional beamforming spectral estimate of a process $s(\boldsymbol{X}, t)$ with Fourier transform $\hat{s}(\boldsymbol{X}; \sigma) = \hat{s}(\boldsymbol{X})$ at frequency σ is

$$S(\boldsymbol{k}; \sigma) = (1/M)^2 \sum_{p,q} \frac{\hat{s}(\boldsymbol{X}p)\,\hat{s}^*(\boldsymbol{X}q)}{|\hat{s}(\boldsymbol{X}p)\,\hat{s}^*(\boldsymbol{X}q)|} \exp i\boldsymbol{k}\cdot(\boldsymbol{X}p - \boldsymbol{X}q).$$

The use of the spectral estimator here is somewhat non-standard, since we are dealing with a deterministic signal rather than a random field of waves. If there is more than one deterministic wave present, the resulting interference pattern will produce a cross-correlation

$$\hat{s}(\boldsymbol{X}p)\,\hat{s}^*(\boldsymbol{X}q)$$

with ripples, and the spectrum S will not be a linear combination of the spectra of the two waves. In the extreme case of two waves with the same magnitude of wavenumber but opposite sign, the spectral estimator will give a peak at zero wavenumber representing a standing wave. However, if a single wave is dominant, the horizontal wavenumber can be extracted. If $s(\boldsymbol{X}, t)$ is a noise-free plane wave of the form

$$\exp \mathrm{i}(\sigma t - \boldsymbol{k}_0 \cdot \boldsymbol{x})$$

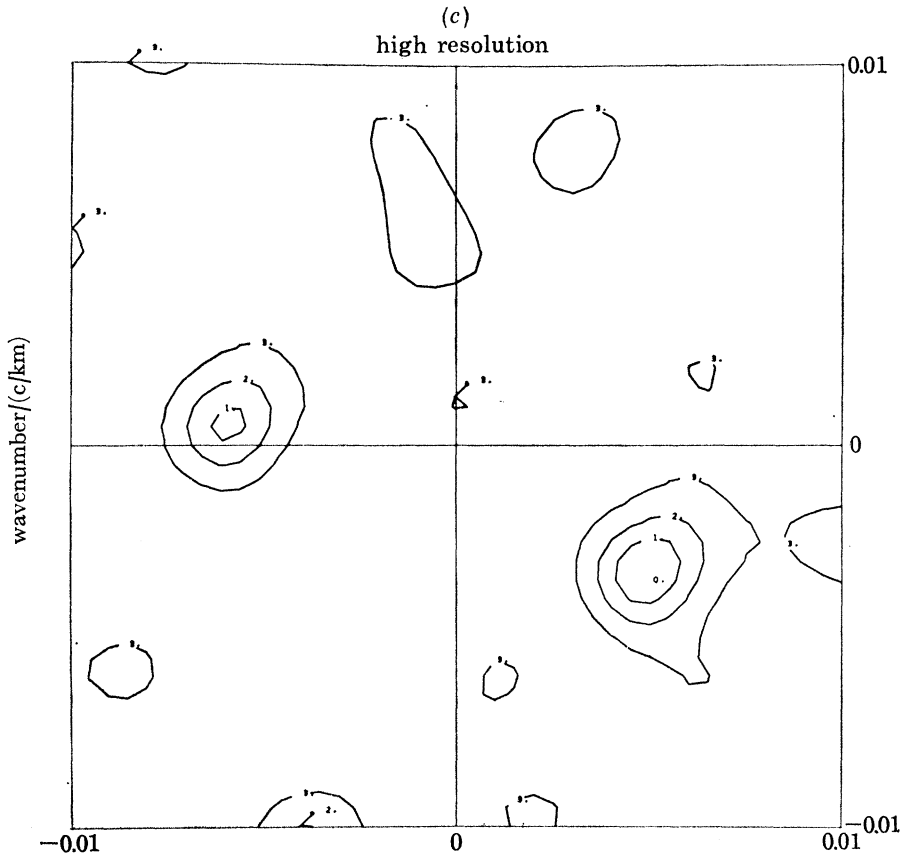

FIGURE 6c. High resolution wavenumber spectral analysis, as above. The peak and sidelobe occur at precisely the same points, but the background has been suppressed.

the beamforming spectral estimation will be just $B(\boldsymbol{k} - \boldsymbol{k}_0)$, and the sidelobes of the central peak evident in figure 6*a* will be reproduced as well as the true peak at $\boldsymbol{k} = \boldsymbol{k}_0$. Figure 6*b* shows the estimate for the first mode M_2 fits. A maximum occurs at $kx = 0.0050$ cycle/km, $ky = -0.0035$ cycle/km in the southeast quadrant, representing a wave with wavelength 163 km propagating towards 125° T. The grid resolution is ± 15 km in wavelength at this wavenumber. The numerical calculation of the M_2 first baroclinic modal wavelength gave 163 km, and the wavenumber spectrum result is thus consistent with the theoretical dispersion relation and the general conclusion of a dominant first baroclinic mode in the M_2 internal tide in this area. A -3 dB relative maximum just above $ky = 0$ in the northwest quadrant is interpreted as a sidelobe of the main peak, from the beam pattern in figure 6*a*. The secondary maximum also gives a wavelength of about 160 km, but if it represented a real wave the interference pattern would place energy at $k = 0$ as we have discussed. Some evidence from the current measurements

which supports the choice of the peak in the southeast quadrant as the physically meaningful one will be discussed later in this section.

A second estimation was also carried out, using the maximum likelihood method (Capon 1969). This is an inverse method in which the data are used to create a filter to pass a plane wave at a given wavenumber but suppress in an optimal sense noise energy at that wavenumber. Figure 6*c* shows the horizontal wavenumber spectrum of the first mode fits according to this estimator. The peak in the southeast quadrant lies at exactly the same grid point as for the conventional estimate, and the side lobe is still present, but the background energy has been reduced.

The amplitudes of the first mode fits varied between 0.9 and 4.4 m, where the normalization used had

$$\int_{-H}^{0} \phi^2(z)\, N^2(z)\, \mathrm{d}z = \bar{N}^2 H$$

$$\bar{N} = (1/H) \int_{-H}^{0} N(z)\, \mathrm{d}z$$

and the weighted integration of the square of vertical displacement $\phi(z)$ is carried out over the water column between the bottom $z = -H$ and the mean free surface $z = 0$. The root mean square amplitude for the fourteen moorings was 3.1 m, representing an average first mode total kinetic plus potential energy density of 0.9×10^2 J/m^2. Multiplying this by the first mode group speed of 2.78 m/s, we derive an energy flux of 0.3×10^3 W/m for the first mode M_2 internal tide, in the direction of wave propagation towards 125° T, since the modal phase and group speeds are in the same sense. The direction of energy flux away from the continental United States suggests that the internal tides observed in MODE are generated there and have maintained their identity while propagating over at least four deep-sea wavelengths. There was no apparent pattern in the spatial distribution of first mode amplitudes; for example, there were no systematic differences between the western part of the array on the abyssal plain and the eastmost areas which were over slightly rougher topography.

Earlier evidence for a deterministic internal tide

During the first part of 1972, several pilot experiments were done in the MODE region. Two earlier moorings with sub-surface flotation, at the site of the MODE-1 central mooring, were also examined to test the general validity of the conclusions drawn here for M_2 internal tides. Table 3 summarizes the results of analyses of temperature records from moorings 421 and 455, using the Woods Hole Oceanographic Institution Buoy Group terminology. There were two temperature records at 1500 m and one from 500 m on these earlier measurements to compare with those from the central mooring. The resulting admittance phases at M_2 frequency in table 3 are not significantly different from those obtained in the main experiment. The coherences of the earlier measurements with the equilibrium tide and the number of 15-day lengths in each case are also given here. The general agreement lends strength to the conclusion that internal waves of M_2 frequency have a deterministic nature in the MODE region. The amplitudes in table 3 do show considerable variation at 500 m, but the variation is not greater than occurred within the group of estimates from individual 15-day lengths at the central mooring during MODE-1 itself.

S_2 internal tides

If we could resolve the S_2 tide in the temperature signals and extract a meaningful first mode signal for the S_2 band, we could directly calculate the group speed $\mathrm{d}\sigma/\mathrm{d}k$ for internal tides. We

have seen that the M_2 band temperature fluctuations have thermocline coherences with the equilibrium tide of about 0.7, so a signal to noise ratio of about unity. The S_2 band temperature fluctuations have about one-third as much energy as the M_2 band, while the S_2 surface tide signal in the MODE region is only 4 % as energetic as the M_2 component (Zetler *et al.* 1975). If we make an assumption that there is a deterministic S_2 internal tide proportional to the surface tide, we can estimate the true coherence of the S_2 band internal tides and the equilibrium tide to be only 0.2 or 0.3, and we do not have enough data to get stable estimates for such a process. This is clearly illustrated by the average temperature-equilibrium tide coherence amplitude distribution in the vertical for the S_2 band in figure 5. As an exercise, the S_2 temperature fluctuations were analysed in the same way as for the M_2 band, modal decomposition carried out, and the wavenumber spectra computed. The higher thermocline coherences for the S_2 fluctuations in figure 5 suggest that some S_2 structure survives, but the wavenumber results were unstable to changes in the number of moorings used for the wavenumber spectral estimates.

TABLE 3. AVERAGE M_2 TEMPERATURE FLUCTUATIONS FROM TWO PREVIOUS SUBSURFACE MOORINGS

(Moorings 421 (28° 00.2′ N, 69° 41.5′ W) and 455 (28° 00.2′ N, 69° 37.6′ W) were deployed in mid-1972, near the central MODE mooring site (27° 59.8′ N, 69° 39.0′ W). A comparison of admittance phases at the 500 and 1500 m levels supports the conclusions drawn from the main experiment. Coherence estimates of temperature and equilibrium tide and the number of 15-day pieces of record involved are given.)

record	depth/m	$10^3 \times$ amplitude/°C	phase/°G	coherence	no. of pieces
4522	514	39.6	201	0.78	3
mooring 1	489	18.6	191	0.68	7
mooring 1	490	19.2	202	0.68	7
4211	1502	4.78	216	0.42	3
4553	1516	6.10	179	0.75	6
mooring 1	1392	4.92	184	0.50	7

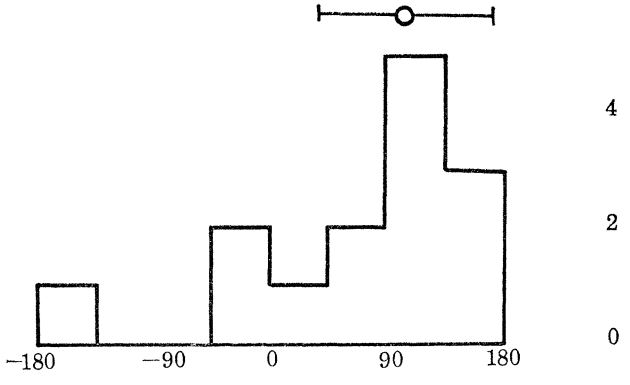

FIGURE 7. Histogram of the phase differences between first mode fits to M_2 and S_2 band temperature fluctuations over 14 of the MODE moorings (°G(S_2) − °G(M_2)). The stability of this measure of the age of the internal tide indicates that there is some determinism in the S_2 internal tide in this area, and since internal waves are dispersive, allows an estimate to be made of the distance travelled by the internal tide since its generation.

However in spite of the low signal to noise ratio in the S_2 band, another approach appears to succeed. Having computed a best fitting first mode at each mooring for the S_2 band, the resulting phase was subtracted from the phase of the corresponding M_2 first baroclinic mode to give a number related to the 'age' of the first mode internal tide at the given mooring. Figure 7 shows

a histogram of the resulting distribution of phase differences across the array. The average difference is 105°, and the distribution is significantly different from a random selection of phases with resulting 95 % confidence phase error bars of about ±45°. Processes which degrade the internal tide signal may act upon M_2 and S_2 waves in the same manner, making the phase differences at a given mooring more stable than the total collection of S_2 phases across the array. The age of the barotropic tide in the MODE region is 32° (Zetler *et al.* 1975), and if we assume that both frequencies of internal tides are generated in the same regions in the same manner, and that the age of the barotropic tide in the effective integrated generation region is similar to the MODE value, then we can relate the increase of about 73° in age to the dispersive nature of oceanic internal waves. For MODE parameters, the age increase for an M_2–S_2 combination related to the horizontal wavenumber $\boldsymbol{k}$ and propagation distance $\boldsymbol{X}$ of

$$\Delta \boldsymbol{k} \cdot \boldsymbol{X}$$

is 73° for $X = 720$ km, where the difference in first mode wavenumbers is 0.18×10^{-2} km^{-1}, and this is entirely consistent with the distance to the steep Blake Escarpment to the west, with the calculated phase error bars suggesting that a more detailed comparison is not called for. In spite of noise problems, the MODE array allows the estimation of both directionality and range of the likely source of internal tides observed in the experiment.

Tidal currents

As previously mentioned, many of the current records were quite short, making a statistical treatment difficult. As well, current measurements were available from at most five depths and from three or less on half the moorings, creating a serious sampling problem. All current records were analysed in the same way as for the temperature records and estimates of coherent tidal energy were made when a given record was long enough to give several 15 day pieces. In general, the M_2 current fluctuations did show significant coherences with the equilibrium tide in the deeper water, but for the thermocline M_2 currents and for all currents in the two adjacent bands, the signal to noise ratio was too low to allow meaningful estimates of coherence with the available data. Using the barotropic plus first two baroclinic modes, we attempted M_2 current modal fits at the two moorings where currents were measured at five levels simultaneously for at least 15 days, and the resulting barotropic estimates, to be discussed later (table 5) are similar. The baroclinic modal fits differ greatly, with an analysis at mooring 1 of currents near the beginning of the experiment showing an energetic first baroclinic mode but a similar analysis for mooring 7 for a time period about three weeks later showing no significant contribution from mode 1. At mooring 1, the first 15 days gave especially energetic M_2 band temperature fluctuations; although we are interested in investigating the statistical nature of the tidal process, we discuss the results from the single 15 days of record at mooring 1. There is no room for wistful thinking in giving the modal decomposition of currents at mooring 1 more statistical weight than the inconclusive analysis at mooring 7, but the case at the central mooring is physically interesting and consistent with the statistical results from the temperature measurements.

Table 4 shows a modal decomposition of M_2 currents at the central mooring for the first 15 days of the experiment, using the barotropic and first two baroclinic modes. For the same 15-day period, the M_2 band temperature fluctuations were especially energetic, giving a first mode displacement amplitude of 4.9 m with phase 014 °G. For the first baroclinic mode, the current ellipse has a major axis of 1.2 cm/s oriented to 160° T, and a minor axis of 0.52 cm/s.

PHILOSOPHICAL TRANSACTIONS OF THE ROYAL SOCIETY A MATHEMATICAL, PHYSICAL & ENGINEERING SCIENCES

The normalization used gives a root mean square current amplitude of 1 cm/s over the whole depth range for unit modal amplitude. The maximum currents flow towards 160° T when the Greenwich epoch G is 174°, above 1300 m, but in the opposite direction below this depth. For a first mode propagating as a single plane wave, the direction of phase propagation is parallel to the major axis of the current ellipse but there is a 180° ambiguity. For the first mode, there is a 180° phase difference between isotherm displacement and the maximum current in the direction of phase propagation, above the node for horizontal current. Simply, for a wave mode with vertical displacement $\phi(z)$, amplitude A, propagating in the X-direction,

$$\zeta = A\phi(z)\cos(\sigma t - kx),$$

$$U = (A\sigma/k)\phi'(z)\cos(\sigma t - kx),$$

$$V = (Af/k)\phi'(z)\cos(\sigma t - kx + \tfrac{1}{2}\pi).$$

TABLE 4. M_2 BAND CURRENT FLUCTUATIONS AT THE CENTRAL MOORING FOR A SINGLE 15-DAY PERIOD

(*Above*, the amplitude and phases of the currents from the five distinct levels available; *below*, the results of a least-squares modal decomposition using a depth independent mode and the first two baroclinic modes. The modes are normalized so that unit amplitude gives unit r.m.s. speed averaged over the entire water column.)

		currents		
depth/m	u/(cm s^{-1})	G_u	v/(cm s^{-1})	G_v
389	2.28	125	3.24	357
391	2.02	126	3.03	002
1392	1.12	067	1.24	303
2916	0.514	140	0.158	235
3963	0.208	174	0.213	196
5356	0.299	141	0.208	201
		modal decomposition		
mode number	u/(cm s^{-1})	G_u	v/(cm s^{-1})	G_v
0	0.66	109	0.62	327
1	0.65	125	1.14	003
2	0.49	167	0.23	012

For the first baroclinic mode, $\phi'(z) < 0$ in the upper part of the water column and ζ and U are 180° out of phase. The current vector (U, V) rotates in a clockwise sense in the northern hemisphere $f > 0$, as noted for the first baroclinic mode derived from mooring 1. The measured isotherm displacement, with phase of 014°G, is 160° out of phase with the southeast major axis of the derived current ellipse, satisfactorily fixing the direction of propagation, and does provide some support for the choice of alias in the wavenumber analysis. The combined current-temperature fit has a first mode horizontal kinetic energy of 0.24×10^3 J/m^2, vertical potential energy of 0.97×10^2 J/m^2, for a ratio of potential to kinetic energy of 0.41 compared to the theoretical ratio of 0.62 for M_2 frequency internal waves at this latitude. The total M_2 band energy is thus nearly four times as great as the estimated average M_2 energy given earlier in this section, and it is assumed that this relatively high energy is the result of a temporal fluctuation which gave a higher signal to noise ratio for the M_2 fluctuations, as well as higher absolute energy levels.

Although the causes of this temporal variation are by no means clear, the variability in the medium through which the internal waves propagate is probably an important factor. Large scale inhomogeneities in the current and density field, due to the mesoscale eddies which MODE was designed to investigate, can refract internal waves and modulate the energy density of propagating wave trains.

Barotropic currents

Because of the simple vertical structure and large horizontal scales of the barotropic component of the tides, we can overcome the noise in the current fields and get stable estimates of the barotropic currents. At the individual moorings with five levels of current measurement, modal fits of M_2 currents gave the results in table 5 for the barotropic mode. Alternatively, since the 200 km horizontal scale of the experiment is a small fraction of the barotropic wavelength, we can treat the whole array as a point and average currents measured at different moorings to gain greater stability. Essentially we use the whole ensemble of current measurements to make a zero vertical and horizontal wavenumber estimate of the semidiurnal tidal current field, by averaging the appropriate Fourier coefficients using admittance phases. Since the averages involve a large number (153) of 15-day pieces, any random noise will be largely filtered out; from the known beampattern of the array, any variation with the horizontal scale of the first baroclinic mode will be largely filtered out in a simple average; and higher modes appear to lack the stability to pose a serious aliasing problem. The vertical averaging will also tend to suppress any baroclinic current fluctuations which survive the temporal and horizontal averaging, and all that remains is the barotropic tide.

TABLE 5. ESTIMATES OF THE BAROTROPIC CURRENTS IN THE THREE SEMIDIURNAL TIDAL BANDS

(Above are the results from least squares fitting of M_2 currents at 5 levels on mooring 1 and mooring 7 for a 15-day record, and the results of Zetler *et al.* (1975) from completely independent estimates. Below are overall averages from the MODE current measurement programme, involving 153 separate 15-day records from all depths and horizontal placements. The coherences between current fluctuations and the equilibrium tide for each band over this ensemble are given. For zero true coherence, 95% of such estimates will be less than 0.14, so although noise levels are high the estimates have considerable significance.)

	M_2 *modal fits*			
	u/(cm s^{-1})	G_u	v/(cm s^{-1})	G_v
mooring 1	0.66	109	0.62	327
mooring 7	0.69	099	0.65	302
Zetler *et al.*	0.49	110	0.80	258

	overall averages					
	u/(cm s^{-1})	G_u	v/(cm s^{-1})	G_v	coherence, u	coherence, v
N_2	0.089	092	0.12	263	0.25	0.22
M_2	0.56	110	0.46	297	0.56	0.45
S_2	0.13	137	0.06	355	0.32	0.13

Table 5 gives the resulting average amplitude and phase for the currents in the three semidiurnal bands, and the calculated coherence between each ensemble and the equilibrium tide. Only the S_2 V-component coherence estimate is less than the 95% confidence limit of about 0.14 for zero true coherence. The M_2 band is highly coherent, and the overall barotropic current estimates agree quite reasonably in both amplitude and phase with the individual modal decomposition estimates in table 5, the current amplitudes in the modal decompositions

being somewhat higher than the overall average which might be expected since there are many fewer degrees of freedom in the modal calculations.

In table 5, the N_2 and S_2 bands show significant coherences in the overall current averages, and the progression in admittance phases among the three constituents mirrors that found in the surface tide in the western North Atlantic (Wunsch 1972). It should be remembered here that the 15-day time window results in only about 50 % of the astronomical N_2 period energy showing up in the nominal N_2 band, and no corrections for this windowing have been applied here. The estimates of barotropic tidal kinetic energy included earlier in figures 3 come from the overall averages here.

Bottom pressure measurements

Recently Zetler *et al.* (1975) made estimates of the barotropic M_2 tide from arrayed bottom pressure gauges in the MODE-1 experiment. Their estimates are included in table 5 for comparison, and the agreement with our results is quite remarkable considering that their measurements needed to resolve differences in pressure the equivalent of 1 cm of sea water in an ambient pressure of 5×10^5 cm. The main discrepancy between the two approaches is in their relatively large V component; it is possible that some of this could be explained by bottom pressure fluctuations due to baroclinic tides coherent with the equilibrium tide, which amount to about 0.3 cm of sea water per cm/s of bottom current for a first baroclinic mode wave, for example.

Using the pressure gauge analyses of Zetler *et al.* and the overall current averages obtained here, we can completely characterize the local behaviour of the M_2 barotropic tide in the MODE-1 area. We find a current ellipse with nearly linear polarization, oriented towards $129°T$ with a major axis of 0.72 cm/s, minor axis 0.043 cm/s, and a clockwise rotation sense. The depth integrated horizontal kinetic energy density of 0.70×10^2 J/m^2 combines with potential energy density of 0.28×10^3 J/m^2 to give a total energy density of 0.35×10^3 J/m^2, and a directly measured horizontal energy flux of 0.25×10^5 W/m towards $317°T$, obtained through the correlation between pressure and current fluctuations. The MODE-1 experiment has thus allowed a rare, perhaps uniquely complete description of the semidiurnal tide in this particular part of the open ocean.

5. Generation of the MODE internal tide

The MODE-1 observations show an M_2 internal tide dominated by the first baroclinic mode. Both the general direction of propagation of the M_2 internal tide towards the southeast, and the weak S_2 signal which allows an estimate of 700 km distance between the effective generation region for the internal tides and the MODE-1 site, suggest the continental margins of the southern United States as the major source of the internal tides observed.

In particular, some 700 km west of MODE centre the ocean depth changes abruptly from near 4800 m on the outlying Blake–Bahama basin to less than 1200 m on the Blake Plateau, with the massive geological fault separating the two provinces called the Blake Escarpment. The slopes on the Escarpment have been estimated to reach 30 degrees from the horizontal or greater (Shepard 1967); the feature itself extends from Cape Hatteras southward about 900 km into the Caribbean, joining the Florida Escarpment and curving to the east along the northern side of the island of Cuba. These steep slopes greatly exceed the average of about 4° found on the continental slopes of eastern North America north of Cape Hatteras (Emery 1965). The step

shelf model of internal tide generation (Rattray, Dworski & Kovala 1969) is well-suited to the Blake Escarpment geometry, since the characteristic slopes determined from the linearized field equations

$$[(\sigma^2 - f^2)/(N^2 - \sigma^2)]^{\frac{1}{2}}$$

are about 4 degrees from the horizontal and much less than the topographic slopes. It is noteworthy that the step shelf models will not apply well to the gentler continental slopes to the north of Cape Hatteras. Aside from the steepness of the Escarpment, this feature is special in the relatively large aspect ratio of shelf depth to deep ocean depth, the 1200 m and 4800 m values giving a ratio 1/4 compared to perhaps 1/20 more characteristic of the continental slopes north of Cape Hatteras. Simple theoretical considerations show that this large aspect ratio favours the generation of low mode internal waves.

From Rattray *et al.* (1969) for example, the amplitude of the nth open ocean baroclinic mode in a constant N step shelf generation model is proportional to $\sin(n\pi H_1/H_2)/(n\pi H_1/H_2)$ for the internal waves forced directly by an incident barotropic tide, where H_1 and H_2 are the shelf and deep ocean depths. Letting Q be the incident volume flux in the barotropic tide, and $\delta = H_1/H_2$, the models show a depth integrated energy density in the deep sea internal tide of

$$(Q^2/H_2) \sum_{n=1}^{\infty} \sin^2(n\pi\delta)/(n\pi\delta)^2 = (Q^2/H_2)(1-\delta)/\delta$$

and a deep sea energy flux of

$$Q^2 N(1 - f^2/\sigma^2)^{\frac{1}{2}} \Sigma \sin^2(n\pi\delta)/(n\pi)(n\pi\delta)^2 \equiv Q^2 N(1 - f^2/\sigma^2)^{\frac{1}{2}} F(\delta),$$

where σ is the tidal frequency, f the Coriolis parameter and the function $F(\delta)$ can be evaluated numerically. These expressions are exact only for a particular antiresonant case in the step shelf models quoted, but contain the main features of the process for all cases. The fraction of seaward tidal energy flux in the first baroclinic mode is then

$$[\sin^2(\pi\delta)/\pi(\pi\delta)^2]/F(\delta)$$

which is a maximum of 95 % for $\delta = \frac{1}{2}$ and vanishes as $\delta \to 0$ or 1. For the constant N case, the first modes for horizontal current are antisymmetric about a point half way between the surface and bottom of the ocean, and the maximum of first mode energy flux when the shelf break has the same shape as the first mode is intuitively reasonable – the internal wave currents must cancel the barotropic current at the vertical cliff. For non-constant N, the modes are not symmetrical in the vertical, but the same considerations will apply. In fact, since the actual first mode calculated for MODE hydrography has a zero in current at about 1250 m depth, with currents above and below this level in opposite directions, the 1/4 aspect ratio of the Blake Escarpment should be especially effective in generating first mode internal waves; simply, the vertical structure of the mode and the topography are similar. Using an estimate $Q = \sigma L \zeta$ for the barotropic volume flux in the M_2 tide at the Blake Escarpment, where $\sigma = 1.4 \times 10^{-4}$ s^{-1} is the M_2 frequency, $L = 500$ km the shelf width and $\zeta = 0.45$ m an estimate of the M_2 surface tide amplitude at the shelf break (Redfield 1958), gives $Q = 0.32 \times 10^2$ m^3/s per m of coastline. With an appropriate constant N of 0.18×10^{-2} s^{-1} and $\delta = \frac{1}{4}$, the simplified generation model predicts a seaward internal wave energy flux of 0.5×10^3 W/m, and of this 0.4×10^3 W/m is in the first mode. This crude theoretical comparison thus gives quite good agreement with the field estimates of 0.3×10^3 W/m in the first baroclinic M_2 wave propagating through the

MODE site, and also confirms theoretical expectations that turbulent dissipation modelled by an eddy viscosity approach would not significantly damp a first mode internal wave at M_2 frequency during its propagation over a 700 km distance (Prinsenberg, Wilmot & Rattray 1974). The ocean between the Blake Escarpment and the MODE site is not disturbed by any marked topography or major currents, as the Gulf Stream remains trapped shoreward of the 800 m line on the continental slope far shoreward of the Blake Escarpment as far north as 33° (Stommel 1958). The combination of simple geometry and a passive environment allows a special relevance of the simple generation models.

Both the theoretical and observed seaward internal tide energy fluxes are less than the M_2 barotropic energy flux of 0.25×10^5 W/m derived in §4 by almost two orders of magnitude. This tends to confirm the conclusion of Wunsch (1975) that the baroclinic tide is not very significant in the overall tidal dissipation budget. However we have seen that the horizontal currents in the internal tide are strictly comparable to those in the barotropic tide, and the unimportance of the internal tide in the energy budget is due to the inefficiency of internal waves as energy carriers (low group speeds) rather than any difference in energy levels.

6. Mooring motion

The *T-P* recorders allowed an evaluation of the effects of mooring motion on measurements of tidal period temperature fluctuations. At the 500 m and 900 m levels pressure recorders were extensively deployed, and about 15 % of the measured temperature variance in the semidiurnal bands could be accounted for by mooring motion. It is necessary to ask if this contamination could affect the coherences between the equilibrium tide and the temperature fluctuations; for example, if the moorings are moved about by barotropic tidal currents, coherent temperature fluctuations could be measured which have nothing to do with internal waves. To examine this question, we calculated the average M_2 band pressure fluctuations for each instrument using averages with respect to the admittance phase, and with the known M_2 barotropic pressure signal subtracted. Multiplying the average pressure fluctuation (equivalent to an average vertical excursion of the instrument) by an appropriate vertical temperature gradient gives a mooring motion induced temperature signal to compare with the actually measured temperatures, also averaged with respect to the equilibrium tide phases. The quotient of mooring motion and measured amplitude of temperature fluctuation gives a figure of noise, and in figures 8*a* and *b* the coherences between the temperature fluctuations in the M_2 band and the equilibrium tide are plotted against this noise indicator. Each point represents an individual instrument, with either 5 or 7 pieces each 15 days long in the average, and separate figures are drawn for cases above 1200 m and those deeper in the water. In general, records showing serious mooring motion also show low coherences, especially the extreme cases in the main thermocline, and we conclude that mooring motion acts to degrade the tidal signals. It is possible for current fluctuations to give a rectified mooring displacement fluctuation, as instruments on a mooring which is vertical on average will always have a downward motion when drag forces act on the mooring, irrespective of the current direction. Thus some of the semidiurnal tidal frequency mooring motion is due to near inertial period currents giving a rectified vertical motion.

Figure 8*a* shows a number of cases of serious mooring motion, including two records where the apparent motion induced signal exceeds the measured signal meaning that some cancellation has occurred. In particular, mooring 6 in the northwest appears seriously affected by mooring

motion, with the two main thermocline instruments with pressure records showing dominant motion-induced temperature signals. This was the worst case, and may have been caused by bursts of strong near-inertial frequency horizontal currents observed in the main thermocline in this area during parts of the experiment. Mooring 6 was excluded from the horizontal wavenumber analysis. It is clear that mooring motion can be a serious experimental difficulty which must be faced in the analysis of measurements obtained from fixed moorings.

7. Summary

The semidiurnal internal tide in the western North Atlantic at the MODE site is dominated by waves generated at the eastern margin of the United States, particularly at the Blake Escarpment 700 km to the west of the site. The steepness and shape of the Escarpment make it

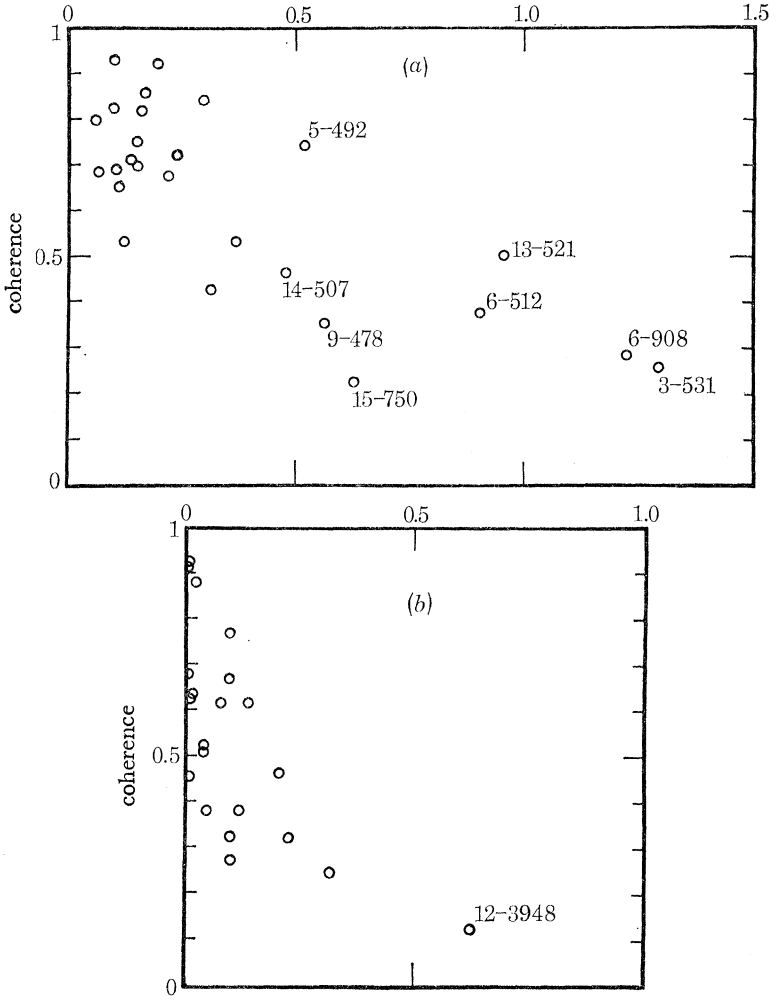

Figure 8*a*. The estimated coherence of M_2 band temperature fluctuations and the equilibrium tide, as a function of the quotient of average mooring-motion-induced temperature fluctuations $\tilde{T}$ and measured temperature fluctuations $\bar{T}$. The averages are done over as many 15-day pieces of record as existed from an individual *T-P* recorder, from depths above 1200 m. Higher average mooring motion gives lower coherences, so the conclusion is that mooring motion will not give falsely high estimates of determinism in the internal tide Some of the points are marked with mooring number and depth of the instrument.

Figure 8*b*. The same for records below 1200 m, showing that in general mooring motion is less serious at the deeper levels.

an effective generator of first mode internal waves, and for the M_2 frequency in particular the waves maintain a simple form while propagating through the MODE area. About 50 % of the M_2 temperature variance in the main thermocline is deterministic, and in principle subject to prediction. The deterministic M_2 internal tide has an estimated energy density of 0.9×10^2 J/m^2, with horizontal currents comparable with the barotropic tide, while the horizontal energy flux in the internal tide is only 1 % as great as the local barotropic energy flux.

The temperature variance spectrum in the vicinity of the M_2 peak is down by a factor of three at a separation of ± 1 cycle per 15 days, and the fluctuations at the neighbouring tidal frequencies are dominated by random internal waves. These may include Doppler shifted M_2 frequency energy and internal waves of non-tidal origin. The deep horizontal currents in the M_2 band are dominated by the barotropic tide, while the neighbouring frequencies, nominally the N_2 and S_2 bands, are dominated by internal waves at all depths. A weak deterministic S_2 internal tide and the dispersive nature of oceanic internal waves allow an estimate of the distance to a common M_2–S_2 effective generation site of 700 km, consistent with the distance to the Blake Escarpment.

Estimates of the barotropic tidal currents for the three major semidiurnal constituents were obtained from the MODE moored currents, in spite of the high internal wave noise levels. From the large body of data collected in MODE, it is evident that the study of oceanic internal tides must be treated as a statistical problem, and that considerable variability in the tidal fields is expected. Mooring motion adds to the experimental difficulties, but its effects are mainly to add incoherent noise to the temperature fluctuations of tidal origin.

The support of the U.S. Office of Naval Research under contracts N00014-67-A-0204-0048 and N00014-75-C-0291-0048 while the author was a student at the Massachusetts Institute of Technology is gratefully acknowledged. Data used in this study was obtained through the efforts of the Woods Hole Oceanographic Institution Moored Buoy Project and the Charles Stark Draper Laboratory, Cambridge, Massachusetts. The MODE-1 field programme was supported by the U.S. International Decade of Ocean Exploration/National Science Foundation and by the Office of Naval Research. Special thanks go to Professor Carl Wunsch, M.I.T., for his guidance through the course of this study. This is MODE contribution 70.

References

Amos, D. E. & Koopmans, L. H. 1963 Tables of the distribution of the coefficient of coherence for stationary bivariate Gaussian processes. Sandia Corporation SCR-483, 327 pp.

Capon, J. 1969 High-resolution frequency-wavenumber analysis. *Proc. I.E.E.E.* **57**, 1408–1418.

Defant, A. 1949 Internal waves and their stability conditions. *Arch. Met. Geophys. Bioklimat.* A**1**, 39–61 (in translation).

Dexter, S., Milliman, J. & Schmitz, W., Jr 1975 Mineral deposition in current meter bearings. *Deep-Sea Res.* **22**, 703–706.

Emery, K. O. 1965 Geology of the continental margin off eastern United States. *Submarine geology and geophysics*, (eds W. F. Whittard & R. Bradshaw), p. 4. London: Butterworths.

Haurwitz, B. 1952 On the reality of internal lunar tidal waves in the ocean, Woods Hole Oceanographic Institution, Tech. Report 52–71.

Hendry, R. 1975 The generation, energetics and propagation of internal tides in the western North Atlantic Ocean, Ph.D. thesis, Massachusetts Institute of Technology and Woods Hole Oceanographic Institution.

MODE Scientific Council 1973 A mid-ocean dynamics experiment. Available from the Department of Meteorology, Massachusetts Institute of Technology (unpublished manuscript).

Munk, W. & Cartwright, D. E. 1966 Tidal spectroscopy and prediction. *Phil. Trans. R. Soc. Lond.* A **259**, 533–581.

PHILOSOPHICAL TRANSACTIONS OF THE ROYAL SOCIETY A MATHEMATICAL, PHYSICAL & ENGINEERING SCIENCES

Munk, W. & Phillips, N. 1968 Coherence and band structure of inertial motion in the sea. *Rev. Geophys.* **6**, 447–472.
Nansen, F. 1902 The Norwegian North Polar Expedition 1893–1896, Scientific Results III, no. 9, London.
Noble, M. 1975 Observations of mid-ocean internal tides during IWEX, MS thesis, Massachusetts Institute of Technology.
Prinsenberg, S. J., Wilmot, W. L. & Rattray, M., Jr 1974 Generation and dissipation of coastal internal tides, *Deep-Sea Res.* **21**, 263–281.
Rattray, M., Jr, Dworski, J. G. & Kovala, P. E. 1969 Generation of long internal waves at the continenta slope. *Deep-Sea Res.* **16** (suppl.), 179–195.
Redfield, A. C. 1958 The influence of the continental shelf on the tides of the Atlantic coast of the United States. *J. mar. Res.* **17**, 432–448.
Seiwell, H. R. 1942 An analysis of vertical oscillations in the southern North Atlantic. *Proc. Am. Phil. Soc.* **85**, 136–158.
Shepard, F. P. 1967 *The Earth beneath the sea*, p. 100. Baltimore: Johns Hopkins Press.
Stommel, H. 1966 *The Gulf Stream*, p. 68. Berkeley: University of California Press.
Wunsch, C. 1972 Bermuda sea level fluctuations in relation to tides, weather, and baroclinic fluctuations. *Rev. Geophys. Space Phys.* **10**, 1–49.
Wunsch, C. 1975 Internal tides in the ocean. *Rev. Geophys. Space Phys.* **13**, 167–182.
Wunsch, C. & Dahlen, J. 1974 A moored temperature and pressure recorder. *Deep-Sea Res.* **21**, 145–154.
Zeilon, N. 1934 Experiments on boundary tides, Goteborgs. *Kengl. Vetensk. Handl.* **5** B, 1–8.
Zetler, B., Munk, W., Mofjeld, H., Brown, W. & Dormer, F. 1975 MODE tides. *J. Phys. Oceanography* **5**, 430–441.

PHILOSOPHICAL TRANSACTIONS OF THE ROYAL SOCIETY A MATHEMATICAL, PHYSICAL & ENGINEERING SCIENCES